Manuscript ID: DOEBTO-UMD-9158-24-JY1

Full Citation: Yang, J., Muehlbauer, J., Tancabel, J., Aute, V., & Hwang, Y. (2024) **Experimentation on Finned-Tube Microchannel Heat Exchanger Incorporating Phase Change Material and R-410A.** *20th International Refrigeration and Air Conditioning Conference at Purdue*, July 15-18, 2024.

Experimentation on Finned-Tube Microchannel Heat Exchanger Incorporating Phase Change Material and R-410A

Jangho YANG, Jan MUEHLBAUER, James TANCABEL, Vikrant AUTE, Yunho HWANG*

Center for Environmental Energy Engineering
Department of Mechanical Engineering, University of Maryland,
College Park, MD 20742, USA

*Corresponding Author: yhhwang@umd.edu

ABSTRACT

Integrating latent heat thermal energy storage, particularly phase change materials (PCM), in building heating, ventilation, air conditioning, and refrigeration (HVAC&R) systems, offers substantial benefits for peak load shifting and energy efficiency. While numerous studies explore PCM-embedded heat exchangers (PCM-HX) using single-phase heat transfer fluids, there needs to be more investigation regarding PCM-HX utilizing two-phase refrigerant flow. This gap is even more pronounced for microchannel heat exchanger (MCHX) configurations. In this study, an MCHX-based PCM-HX was built and tested to analyze and evaluate the performance of a PCM-HX operating with a two-phase refrigerant as the working fluid. A commercially available MCHX condenser unit was embedded with 2.6 kg of RT35 PCM and tested using R-410A as the working fluid, using an in-house test loop to control the refrigerant inlet conditions precisely. Thin and minimally invasive T-type thermocouples traced the temperature evolution along MCHX channels and tube banks. Additional larger T-type thermocouple probes at the refrigerant inlet and outlet measured the average power of the PCM-HX during condensing tests, ranging from 0.7 kW to 1.6 kW based on mass flow rates varying from 3.5 g/s to 8 g/s. This experimental study on MCHX-based PCM-HX with a two-phase refrigerant has the potential to offer practical design guidelines for the direct integration of PCM-TES in HVAC&R systems without the use of a secondary loop, while caution is advised to avoid a substantial increase in the refrigerant charge amount.

1. INTRODUCTION

Thermal energy storage (TES) systems can be applied across diverse building heating, ventilation, air conditioning, and refrigeration (HVAC&R) systems. These systems offer numerous advantages in heating or cooling systems depending on their operational modes, including the ability to shift peak energy demand, leverage off-peak electricity rates, and sometimes improve the coefficient of performance (COP) (Ermel et al., 2022; Song et al., 2018; Souayfane et al., 2016), particularly in heating or cooling systems depending on their operational modes. Numerous studies have explored and discussed various PCM-embedded heat exchanger (PCM-HX) configurations to integrate them into potential HVAC&R applications, with most focusing solely on single-phase fluid as the preferred heat transfer fluid in the tube side. Choure et al. (2023) reviewed various methods of heat transfer enhancement techniques for PCM-HX-based TES systems, albeit focusing on water as the heat transfer fluid (HTF). While there is limited literature on studies utilizing two-phase refrigerant as HTF, Qiao et al. (2019) conducted an experimental study on PCM-HX used in a personal cooling device with R-134A as the chosen HTF, emphasizing a system-level analysis and comparing different copper tube-based in-house HX configurations and PCM-side heat transfer enhancement techniques. Khalifa and Koz (2016) numerically investigated the solidification process of a serpentine-shaped PCM-HX evaporator in a

vapor compression refrigeration system using a quasi-2D model, but experimental validation with an actual two-phase refrigerant was not conducted; water was instead utilized as the HTF.

To bridge the gaps in previous studies, this research aims to experimentally investigate a commercially available aluminum finned-tube microchannel heat exchanger (MCHX) embedded in PCM for refrigerant condensing (PCM melting) tests, conducting a detailed component-level study for performance evaluation. The results of these tests can offer insights into the potential use of PCM-HX with a two-phase refrigerant as a heat transfer fluid (HTF) in HVAC&R applications without the need for a secondary loop with a single-phase HTF. Additionally, the dataset generated can be used for potential validation of simulation models in the future.

2. EXPERIMENT DESCRIPTION

2.1 Two-Phase Refrigerant-to-PCM Test Facility

The schematic diagram of the test facility with R-410A as a selected HTF, shown in Figure 1-(T), comprises three main sections: the PCM-HX section, the refrigerant cart section, and the water/glycol section. The outdoor chiller, alongside automatically controlled diverging valves and an immersive heater, ensures precise temperature control of the water/glycol tank. This, in turn, regulates the temperature of the oversized condenser and its system pressure. The oversized condenser's substantial refrigerant volume allows it to function effectively as a large receiver, facilitating this temperature and pressure control of the system loop. Heat exchange within the water/glycol loop and its connected components is facilitated by plate HXs and circulation pumps. A small chiller cools the subcooler HX after the oversized condenser to prevent the refrigerant pump from running dry. The refrigerant flows through the mass flow meter and is heated to the desired target temperature before entering the PCM-HX test section. Initially, the refrigerant can bypass the main PCM-HX loop until the desired inlet conditions are achieved, controlled by solenoid valves. Once conditioned to target values, the solenoid valves open the PCM-HX loop, allowing the refrigerant to exchange heat with the PCM-HX before exiting. An in-line post heater is positioned after the PCM-HX outlet to superheat the refrigerant if it exits the PCM-HX in the two-phase region. This process enables the back-calculation of the specific enthalpy of the refrigerant at the PCM-HX outlet. The watt meter records the power input of the post heater. Finally, the refrigerant re-enters the oversized condenser to initiate the loop once again. It is worth noting that a back pressure valve, which is installed to ensure stable system pressure in case of pressure control issues during an evaporator test, was not utilized in this study as only the condensing test was conducted.

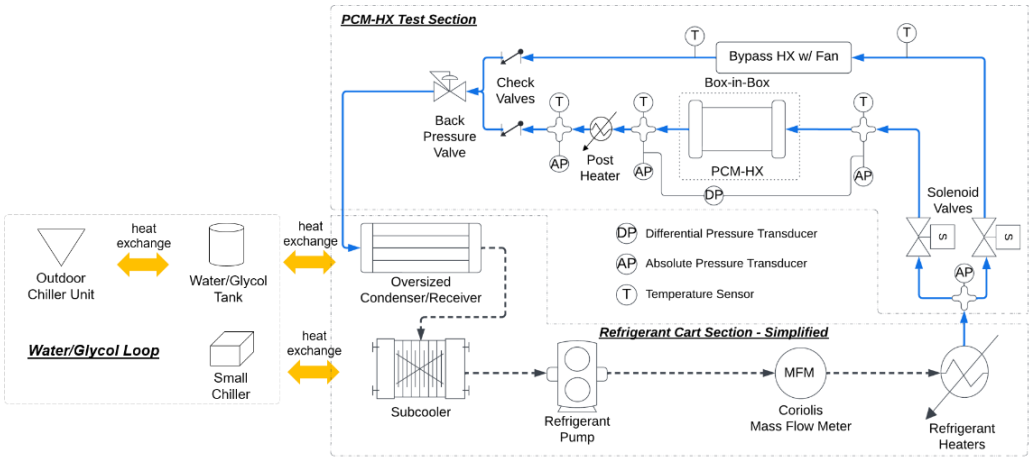

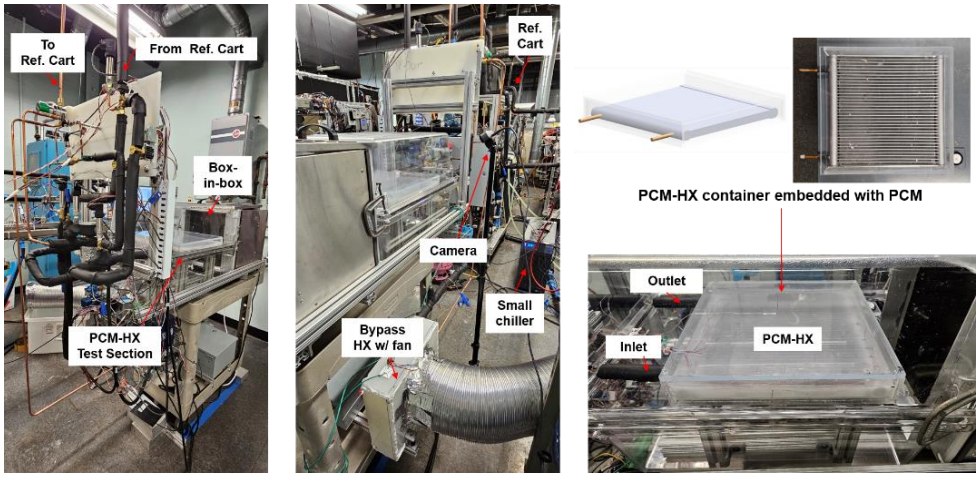

Figure 1: (Top) Two-phase refrigerant-to-PCM test facility overview;
(Bottom) Images of two-phase refrigerant-to-PCM test facility.

Images of the PCM-HX test section and a portion of the refrigerant cart are shown in Figure 1-(B). It is important to highlight that the PCM-HX is enclosed within a local chamber capable of regulating temperatures ranging from 30°C to 80°C. This controlled environment allows for adjustment of initial temperature conditions for the PCM-HX, a setup referred to as a "box-in-box" configuration. The primary function of the local chamber is to pre-melt the PCM for conducting an evaporator test. Thus, for the condenser test in this study, the local chamber was utilized to provide a stable environment where temperature fluctuations were minimized compared to the outside room temperature.

2.2 PCM Properties and PCM-HX Configuration

The PCM selected for the experiment was RT35 (RT35 Data Sheet, 2020). Table 1 displays the manufacturer's property data. The measured mass of the embedded PCM within the container was recorded as 2.6 kg.

Table 1. RT35 thermophysical properties (RT35 Data Sheet, 2020)

Nominal Phase Change Temperature [°C]	35
Density [kg/m^3]	860 [solid], 770 [liquid]
Thermal Conductivity [W/m-K]	0.2 [solid], 0.2 [liquid]
Specific Heat [kJ/kg-K]	2 [solid], 2 [liquid]
Heat Storage Capacity [kJ/kg] (Sensible + Latent Heat, 26°C – 41°C)	160 (with ±7.5% accuracy)

The PCM-HX details are illustrated in Figure 2. A commercially-available aluminum MCHX with louvered fins (349 mm x 332 mm, W x H) was selected, and its refrigerant flow path is depicted in Figure 2-(L). Thermocouples were installed on both the header side (yellow) and tube side (red), as shown in Figure 2-(M). Thin T-type thermocouples were used, and silver epoxy was applied to permanently attach them to the HX surfaces. Figure 2-(R) provides a side view of the outlet-side corner, highlighting the locations of thermocouples used to determine the end of PCM melting. Two thermocouples were strategically placed at the bottom side of the outlet corner, as this area was anticipated to be the last portion inside the container to undergo melting. These thermocouples serve to indicate the completion of the PCM full melting process by monitoring their temperatures. The outer container, constructed from acrylic plates, features approximately 5 mm gaps between the HX and the inner walls. This design facilitates more convenient simulation validation in the future, ensuring uniform physical boundaries.

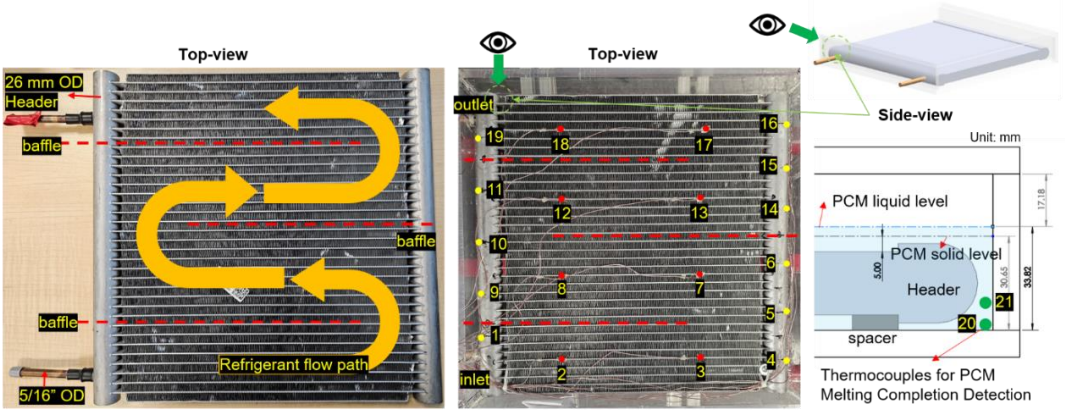

Figure 2: (Left) HX configuration; (Middle) Installed thermocouple locations; and (Right) A side view of the container with melting completion determining thermocouple locations.

3. DATA REDUCTION

The measured values acquired from the installed thermocouples and absolute pressure transducers at the inlet and outlet of the PCM-HX, as well as at the outlet of the post heater, were employed to determine the specific enthalpy values of R-410A under diverse conditions. Furthermore, the Coriolis mass flow meter was utilized to measure the refrigerant mass flow rate, aiding in the calculation of instantaneous power from the PCM-HX. When the inlet condition of the refrigerant is consistently conditioned as superheated vapor, and the refrigerant outlet is in the subcooled liquid region, the power can be calculated using Equation (1).

$$\dot{q}_{1P} = (h_{HX,in} - h_{HX,out}) \cdot \dot{m} \tag{1}$$

If the outlet condition is in the two-phase region, the refrigerant undergoes superheating by a post heater after exiting the PCM-HX. A specific enthalpy value at the post heater outlet can be determined using the post heater outlet temperature and absolute pressure measurements. Subsequently, to back-calculate the specific enthalpy value of the (two-phase) PCM-HX outlet, the post heater power as measured from a watt meter, along with the mass flow rate, are utilized as in Equation (2). The power can then be calculated using Equation (3).

$$h_{HX,out,2P} = h_{PH,out} - \frac{\dot{q}_{PH}}{\dot{m}} \tag{2}$$

$$\dot{q}_{2P} = (h_{HX,in} - h_{HX,out,2P}) \cdot \dot{m} \tag{3}$$

The accumulated energy from the refrigerant during the test can be calculated using Equation (4), with each interval set to a time step of 10 seconds for this study.

$$E_{R-410A} = \int \dot{q}_{R-410A}\, \Delta t \tag{4}$$

The state of charge (SOC) of PCM-HX was defined as in Equation (5).

$$SOC = \frac{C_{max} - E_{R-410A}}{C_{max}} \cdot 100 \tag{5}$$

The useful maximum capacity of the PCM-HX is defined by Equation (6), which takes into account the sensible energy from the PCM in the solid phase, the latent energy of the PCM, and the thermal mass of the aluminum MCHX, as calculated by Equations (7)-(9), respectively. It is important to note that the sensible energy from the PCM in the liquid phase was not included in the useful maximum capacity of the PCM-HX, as the primary focus is on the energy harvested from the PCM phase change process (melting) starting from the initial solidified PCM inside the container.

$$C_{max} = Q_{PCM,s} + Q_{PCM,l} + Q_{HX,TM} \tag{6}$$

$$Q_{PCM,s} = c_{P,PCM} \cdot m_{PCM} \cdot (26^{\circ}C - T_{ini.}) \tag{7}$$

$$Q_{PCM,l} = m_{PCM} \cdot (\Delta H_{PCM}) \tag{8}$$

$$Q_{HX,TM} = c_{P,HX} \cdot m_{HX} \cdot (41^{\circ}C - T_{ini.}) \tag{9}$$

Finally, the power density, energy density, specific power density, and specific energy density of the PCM-HX, were defined by Equations (10)-(13), respectively. It is important to note that the average power and accumulated energy values considered here only account for the portion where the refrigerant outlet condition was in the subcooled liquid region. This is because the effectiveness of the PCM-HX diminishes significantly when the exiting refrigerant is in the two-phase or superheated region.

$$\dot{q}_d = \frac{\dot{q}_{1P,avg.}}{V_{PCM-HX}} \quad (10) \qquad E_d = \frac{E_{R-410A,1P}}{V_{PCM-HX}} \quad (11)$$

$$\dot{q}_{sp} = \frac{\dot{q}_{1P,avg.}}{m_{PCM-HX}} \quad (12) \qquad E_{sp} = \frac{E_{R-410A,1P}}{m_{PCM-HX}} \quad (13)$$

4. RESULTS AND DISCUSSION

4.1 Test Conditions

Table 2 summarizes the test conditions conducted in this study. "Initial T" represents the average initial temperatures from the installed thermocouples inside the PCM-HX, which correspond to the ambient temperature. "Avg. Inlet T" and "Avg. Inlet P" denote the average temperature and pressure values of the refrigerant inlet conditions until the PCM inside the container is fully melted. "Avg. Inlet Condensing T" represents the average saturated liquid temperature value based on the measured pressure values at the PCM-HX inlet. The inlet condition of R-410A into the PCM-HX was adjusted to simulate the compressor discharge for a typical residential air-conditioning application.

Table 2. Test conditions under different mass flow rates.

MFR [g/s]	Initial T [°C]	Avg. Inlet T [°C]	Avg. Inlet P [kPa]	Avg. Inlet Condensing T [°C]
3.5	24.6	59.6	2907.7	47.6
4	25.3	59.9	2922.1	47.9
4.5	24.9	60.2	2934.6	48.0
5	25.3	60.1	2936.6	48.1
5.5	25.6	60.6	2949.4	48.3
6	25.0	60.5	2959.7	48.4
8	24.3	60.4	2986.8	48.9

4.2 Test Results and Observations

Figure 3-(L) shows a plot of the measured power and accumulated energy from R-410A during the condensing tests. A higher mass flow rate corresponded to a higher power and caused the refrigerant to transition more quickly to the two-phase region. This was evidenced by the significant decrease in power following the initial stable power supply pattern. Consequently, the slope of the accumulated energy became more shallow as the power decreased, reflecting the outlet being two-phase R-410A. It should be noted that the staircase-like patterns correspond to times when the post heater was manually controlled to superheat the refrigerant. This resulted in a back-calculation of the refrigerant outlet condition. In simpler terms, when the power input from the post heater was reduced, the back-calculation occurred instantaneously, while the temperature change at the post heater outlet lagged behind due to the thermal mass of the heater.

Figure 3-(R) illustrates the measured inlet, measured outlet, and computed outlet condensing temperature of the refrigerant from the PCM-HX. Notably, the 3.5 g/s test condition exhibits abnormal inlet temperature fluctuations during the first 15 minutes of the test, which was suspected to be caused by insufficient refrigerant flow to properly contact the thermocouple probe in the cross-fitting. By examining the outlet temperature and condensing temperature, we can observe the timing of the refrigerant entering the two-phase region as discussed above in Figure 3-(L). Moreover, the higher mass flow rate tests showed the outlet temperature exceeding the condensing temperature, i.e., superheated outlet refrigerant before 30 minutes. A slight bump in condensing temperature was observed as the outlet temperature approached the condensing temperatures, likely due to the increasing temperature of the refrigerant entering the oversized condenser, eventually surpassing the water/glycol tank temperature, and thereby slightly elevating the refrigerant pressure inside the oversized condenser. This minor issue can be addressed in the future by installing an additional subcooler before the oversized condenser to cool the refrigerant before entering.

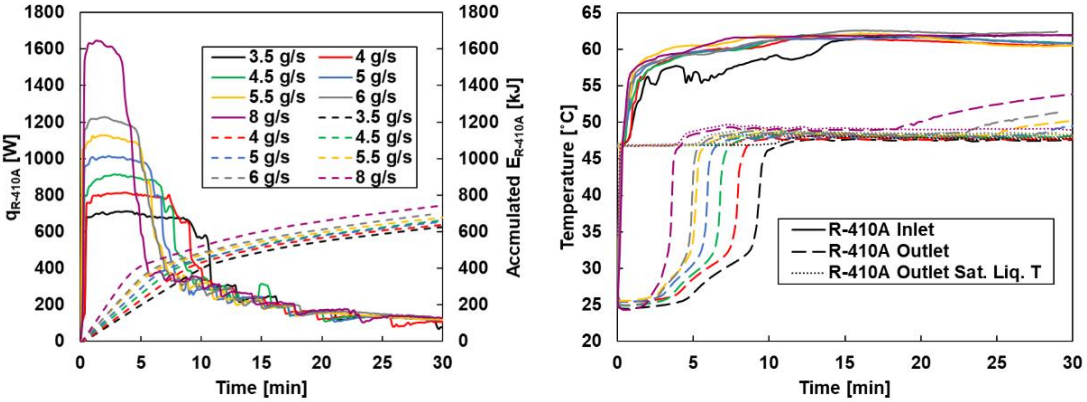

Figure 3: (Left) Measured power and accumulated energy from R-410A;
(Right) Measured R-410A inlet, outlet, and outlet condensing temperatures

Figure 4-(L) shows the comparison between the time taken for R-410A to reach the two-phase condition and the time required for full PCM melting inside the container. A significant discrepancy between these two values is evident, indicating that portions of the PCM volume were not fully utilized before the R-410A outlet entered the two-phase region. This discrepancy is likely attributed to the PCM volume located in the gap area between the HX surfaces and the container inner wall. This gap volume, which was not in the vicinity of the HX surfaces, accounted for approximately 27% of the total PCM volume embedded inside the container. Therefore, minimizing this gap volume is crucial in practical applications to maximize PCM utilization within a short period.

Figure 4-(R) presents the recorded temperatures from selected thermocouples on the PCM-HX surface during the 4 g/s mass flow rate test. The temperatures from both the bank and tube side indicated a gradual increase along the MCHX fluid flow path. Notably, TC10 and TC19 exhibited a rapid temperature increase at the beginning, possibly attributed to heat transfer along the headers from neighboring banks.

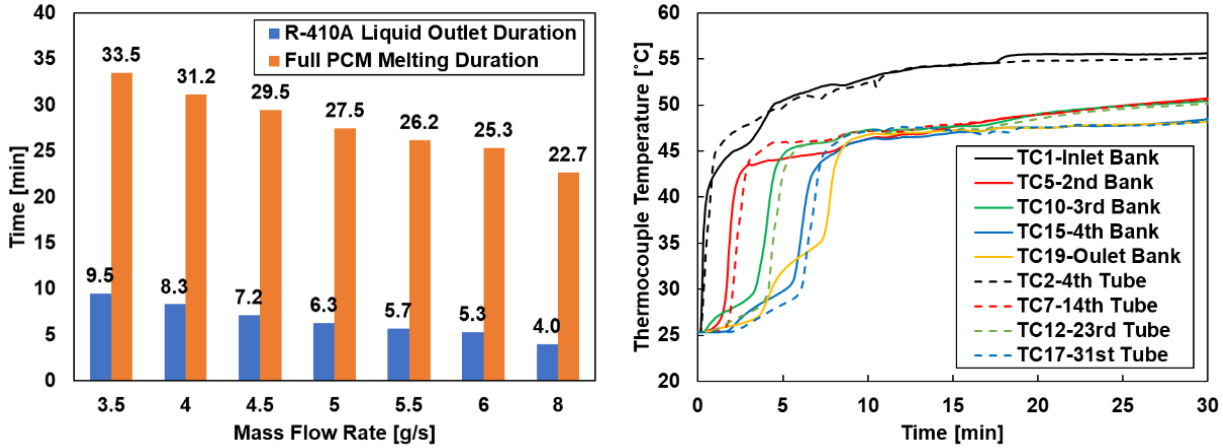

Figure 4: (Left) Test duration up to R-410A subcooled liquid outlet condition only and up to full PCM melting;
(Right) Temperature plots of the selected thermocouples on the PCM-HX surfaces from the 4 g/s test.

Figure 5 shows a time-lapse of the PCM melting process as captured by the camera setup during the 4 g/s mass flow rate test. The melting progression was observed to follow the MCHX refrigerant flow path. Additionally, it was clear that the PCM located away from the HX surface melted last. The recorded thermocouple temperatures and images of the PCM-HX melting process can serve as valuable validation datasets for future simulations of PCM-HX melting with two-phase refrigerant flow.

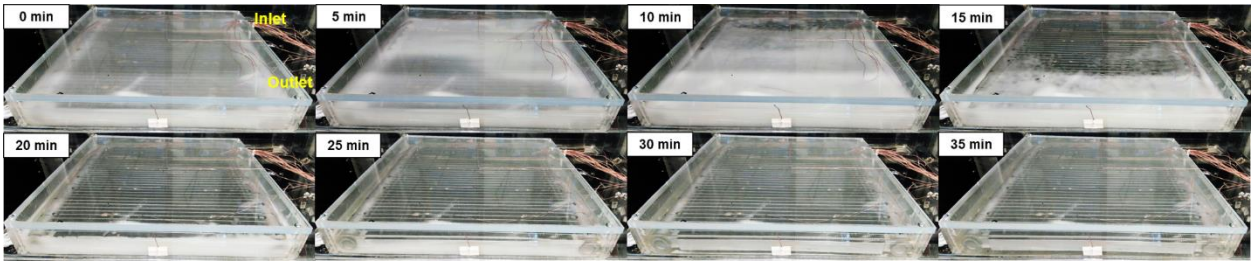

Figure 5: Visual observation of the PCM-HX from the 4 g/s test.

4.3 Rate Capability and Ragone Plots

To further assess the PCM-HX performance, we utilize an approach outlined by Woods et al. (2021) to generate rate capability curves and Ragone plots. In Figure 6-(L), the rate capability curves between SOC and the refrigerant outlet temperature are depicted. Here, the cutoff temperature line is arbitrarily set as the near-condensing temperature of the refrigerant to illustrate the concept of rate capability curves. The cutoff temperature of the thermal energy storage (TES) is generally application specific and is defined to gauge the extent of useful energy utilization (i.e. higher cutoff temperatures for heating applications and lower cutoff temperatures for cooling applications). In this study, the PCM-HX was fabricated for a general performance assessment, and thus the cutoff temperature was chosen as the near-condensing temperature of the refrigerant, as this corresponds to the time when the majority of the PCM state of charge is depleted. Typically, the plot becomes more informative when curves of significantly different shapes are observed, indicating varying performance across different mass flow rates reaching the cutoff lines in distinct ways. However, with the available data covering mass flow rates ranging from 3.5 g/s to 8 g/s, the curves do not exhibit significant differences in this context. This suggests that the PCM-HX capacity is too large for the selected mass flow rates to yield meaningful distinctions among the data points. However, it is worth noting that tests with higher mass flow rates beyond 8 g/s were not feasible with the current experimental setup due to limitations in the post heater capacity.

With the same principle in mind, Figure 6-(R) illustrates the rate capability curves plotted against SOC and time. In this scenario, if an application specifies a cutoff time, one can discern which test condition proves most effective for the given time frame. It is important to note that the times at which the maximum capacity of the PCM-HX is reached (0% SOC) differ significantly from the durations required for complete PCM melting (Figure 4-(L)), which seems counterintuitive. This disparity arises because the accumulated energy measured from R-410A includes the thermal mass of the acrylic plates and heat loss to the surroundings, while the estimated maximum capacity of the PCM-HX considers only the PCM capacity and the MCHX thermal mass. This discrepancy could be addressed in the future by measuring the thermal mass of the container and implementing robust insulation.

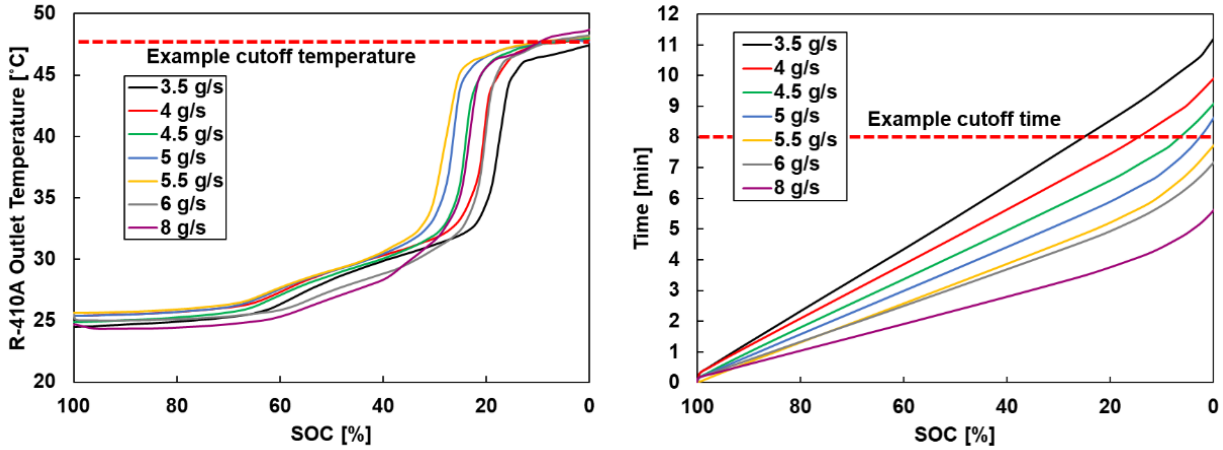

Figure 6: Rate capability plots: (Left) R-410A outlet temperature vs. SOC; (Right) time vs. SOC.

Figure 7 presents the Ragone plots, which illustrate the PCM-HX performance under various mass flow rates, considering average power and accumulated energy values only for the segment where the refrigerant outlet condition remained in the subcooled liquid region. As previously noted, the capacity of the MCHX is too large for the tested

mass flow rates. Consequently, the curve ascends vertically rather than trending towards the upper left corner as the mass flow rate increases, as achieving near 0% SOC is possible regardless of the mass flow rate. Ideally, to pinpoint the optimal operating condition of the PCM-HX with the most favorable balance between power and energy, a reference data point in red, as shown in Figure 7-(L), is necessary. This data point demonstrates a noticeable shift towards the upper left corner compared to the nearly vertical curve observed with the low mass flow rate data points, indicating an increase in power but less utilization of energy. Therefore, the data point preceding this reference point is likely the optimal operating condition, showcasing high power output while almost fully utilizing the PCM-HX capacity.

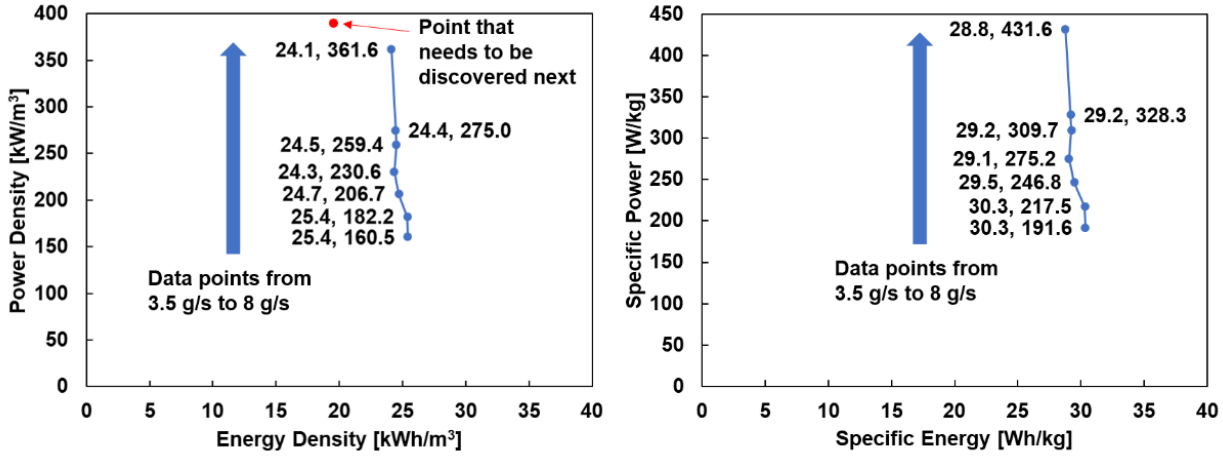

Figure 7: Ragone plots: (Left) power density vs. energy density; (Right) specific power vs. specific energy.

4.4 Potential Application – Heat Pump Defrost Cycle

Given the observed characteristics of the test results and the performance of the fabricated PCM-HX, a potential application for integrating PCM-HX can be identified. The PCM-HX in this study utilizes phase transitions from both the PCM and refrigerant sides and efficiently delivers all energy within a short time frame. Therefore, integrating the PCM-HX TES into a heat pump defrost cycle could be a viable concept. Figure 8-(L) illustrates the heat pump operation mode of the proposed concept, wherein a portion of the refrigerant from the compressor discharge is directed to the PCM-HX by controlling the flow control valve to pre-melt the PCM while simultaneously delivering hot air to an indoor environment. It is important to note that by controlling the solenoid and flow control valves, the compressor discharge can be directed solely through either the condenser or the PCM-HX depending on various scenarios, e.g., (i) the PCM-HX is fully charged (melted) and no refrigerant needs to be diverted, or (ii) rapid PCM melting is required during periods of heat pump inactivity. As shown in Figure 8-(R), during the defrosting operation, the refrigerant flow is reversed, and the PCM-HX functions as an evaporator, thereby preventing the release of cold air indoors. Furthermore, utilizing the PCM melting temperature compared to the indoor return air temperature improves overall cycle efficiency by reducing temperature lift, i.e., the elevation in temperature increases the evaporating pressure, thereby reducing the workload on the compressor. Using the PCM-HX performance data presented herein, the PCM-HXs can be sized and connected in parallel to fulfill the defrosting capacity requirements for a given system. It must be emphasized that it is essential to select the minimal total HX volume available while meeting the operational requirements to minimize the total added refrigerant charge to the system. This application holds promise for the studied PCM-HX, as rapid charging and discharging processes are essential for effective defrosting.

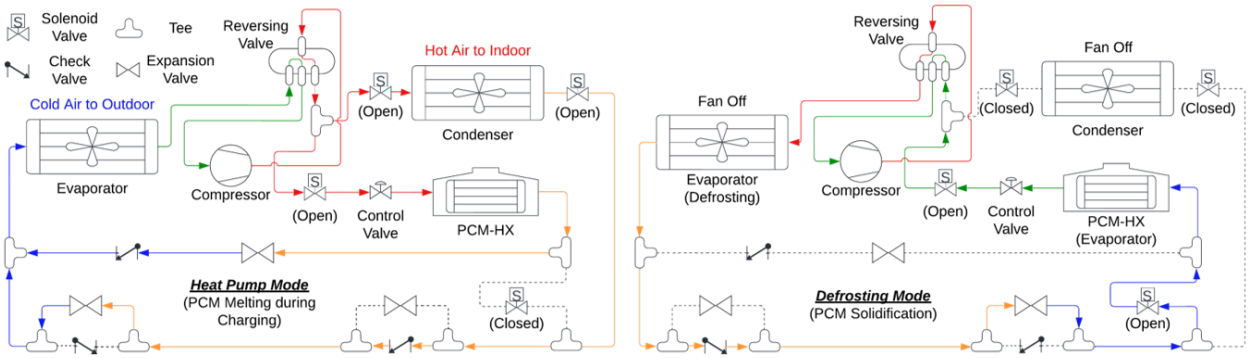

Figure 8: Schematic diagram of a conceptual heat pump loop integrated with PCM-HX TES: (Left) Heat pump operation mode; (Right) Defrosting operation mode.

5. CONCLUSION

A commercially-available aluminum MCHX was embedded in PCM and tested as a PCM-HX TES where the working fluid was a two-phase (condensing) refrigerant with mass flow rates ranging from 3.5 g/s to 8 g/s. The PCM-HX demonstrated a consistent increase in power from 0.7 kW to 1.6 kW as the mass flow rate increased, yet achieved nearly identical energy utilization up to a cutoff (condensing) temperature, suggesting the need to explore higher mass flow rates beyond 8 g/s to identify the optimal operating condition as per rate capability and Ragone plots. The measured temperatures from thermocouples installed on the PCM-HX surfaces, along with images obtained from the camera setup, will provide a valuable dataset for simulation validation in the future. Based on the investigated PCM-HX, a potential application is suggested: a defrosting method for a heat pump system. Future work includes conducting refrigerant evaporating (PCM solidification) tests, conducting comparison tests using water as the working fluid, and performing a detailed techno-economic analysis of the suggested defrosting application concept, which could be beneficial for future research endeavors.

NOMENCLATURE

C	capacity	(kJ)
c_P	specific heat	(kJ/kg-K)
E	accumulated energy	(kJ)
h	specific enthalpy	(kJ/kg)
ΔH	heat storage capacity	(kJ/kg)
m	mass	(kg)
$\dot{m}$	mass flow rate	(kg/s)
$\dot{q}$	power	(W)
Q	energy	(kJ)
SOC	state of charge	(%)
Δt	time step	(s)
V	volume	(m^3)

Subscripts

avg.	average
d	density
HX	heat exchanger
in	inlet
ini.	initial
l	latent
max	maximum
out	outlet
PH	post heater
s	sensible
sp	specific
TM	thermal mass
1P	single-phase
2P	two-phase

REFERENCES

Choure, B. K., Alam, T., & Kumar, R. (2023). A review on heat transfer enhancement techniques for PCM based thermal energy storage system. *Journal of Energy Storage*, *72*, 108161. https://doi.org/10.1016/j.est.2023.108161

Ermel, C., Bianchi, M. V. A., Cardoso, A. P., & Schneider, P. S. (2022). Thermal storage integrated into air-source heat pumps to leverage building electrification: A systematic literature review. *Applied Thermal Engineering*, *215*(July), 118975. https://doi.org/10.1016/j.applthermaleng.2022.118975

Khalifa, H. E., & Koz, M. (2016). Numerical Investigation of the Freezing of a Phase Change Material in a Thermal Storage Device With an Embedded Evaporator. *Proceedings of the ASME 2016 Heat Transfer Summer Conference collocated with the ASME 2016 Fluids Engineering Division Summer Meeting and the ASME 2016 14th International Conference on Nanochannels, Microchannels, and Minichannels*, Washington, DC, USA. July 10–14, 2016. V002T08A021. https://doi.org/10.1115/HT2016-7409

Qiao, Y., Du, Y., Muehlbauer, J., Hwang, Y., & Radermacher, R. (2019). Experimental study of enhanced PCM exchangers applied in a thermal energy storage system for personal cooling. *International Journal of Refrigeration*, *102*, 22–34. https://doi.org/10.1016/j.ijrefrig.2019.03.006

RT35 Data Sheet. (2020). Rubitherm Technologies. https://www.rubitherm.eu/media/products/datasheets/Techdata_-RT35_EN_09102020.PDF

Song, M., Niu, F., Mao, N., Hu, Y., & Deng, S. (2018). Review on building energy performance improvement using phase change materials. *Energy and Buildings*, *158*, 776–793. https://doi.org/10.1016/j.enbuild.2017.10.066

Souayfane, F., Fardoun, F., & Biwole, P. H. (2016). Phase change materials (PCM) for cooling applications in buildings: A review. *Energy and Buildings*, *129*, 396–431. https://doi.org/10.1016/j.enbuild.2016.04.006

Woods, J., Mahvi, A., Goyal, A., Kozubal, E., Odukomaiya, A., & Jackson, R. (2021). Rate capability and Ragone plots for phase change thermal energy storage. *Nature Energy*, *6*(3), 295–302. https://doi.org/10.1038/s41560-021-00778-w

ACKNOWLEDGEMENT

This material is based upon work supported by the U.S. Department of Energy's Office of Energy Efficiency and Renewable Energy (EERE) under the Building Technologies Office (BTO) Award Number DE-EE0009158. The views expressed herein do not necessarily represent the views of the U.S. Department of Energy or the United States Government. This work was also supported in part by the Modeling & Optimization Consortium and Energy Efficiency & Heat Pumps Consortium at the Center for Environmental Energy Engineering at the University of Maryland. The authors would like to acknowledge Y. Shabtay and J. Black of Heat Transfer Technologies, LLC, for their manufacturing expertise which contributed to the production of the HX prototype studied in this work.